**Supplementary information**

# Width-Dependent Electronic and Magnetic Properties of Penta-$PdSe_2$ Nanoribbons: A First-Principles Study

Zixin Jiao,[a,b] Zhengyuan Liu,[a,b] Zhenquan Tan[*b] and Lizhao Liu[†a]



[a.] *School of General Education, Dalian University of Technology, Panjin 124221, P. R. China*
[b.] *Leicester International Institute, Dalian University of Technology, Panjin 124221, P. R. China*
[*] tanzq@dlut.edu.cn;
[†] lizhao_liu@dlut.edu.cn.

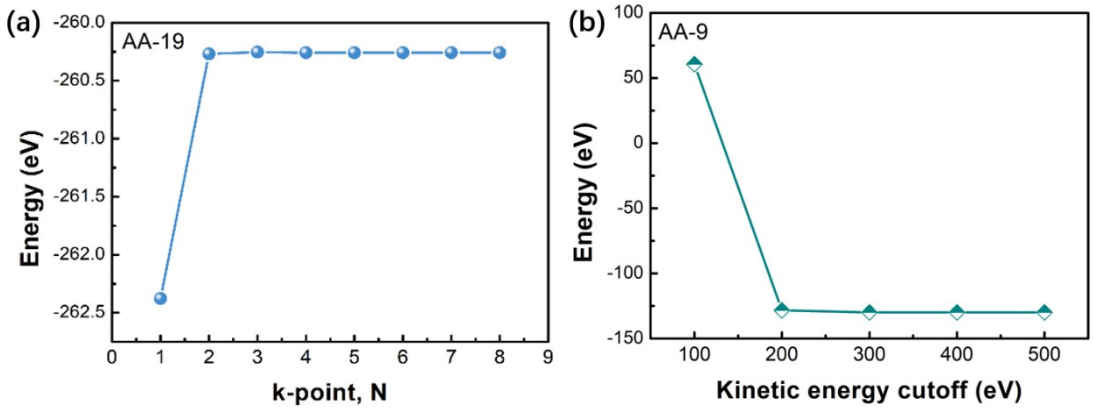


**Fig. S1.** Testing calculations to show the convergence of total energy of AA-19 and AA-9 nanoribbons with respect to (a) k-point mesh (N×1×1) and (b) kinetic energy cutoff.

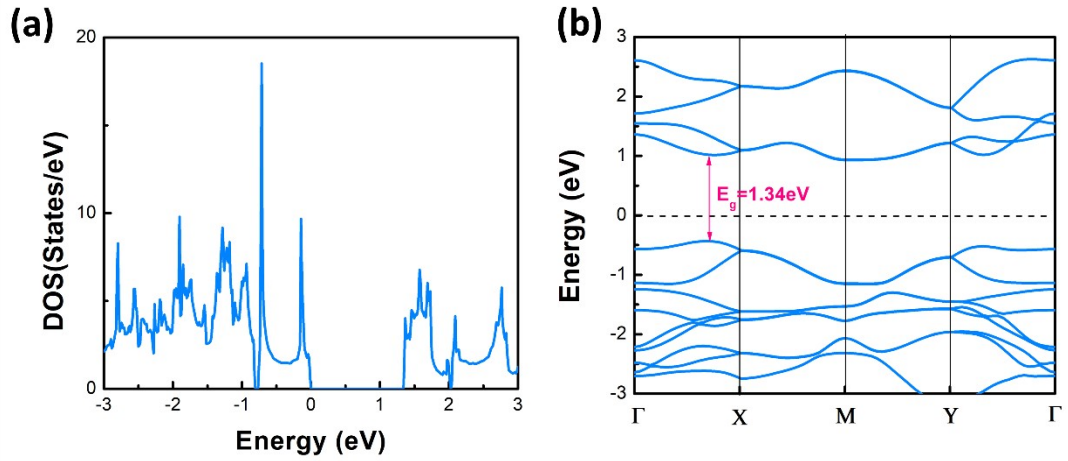


**Fig. S2.** (a) DOS and (b) band structure of monolayer penta-$PdSe_2$ calculated by PBE function.

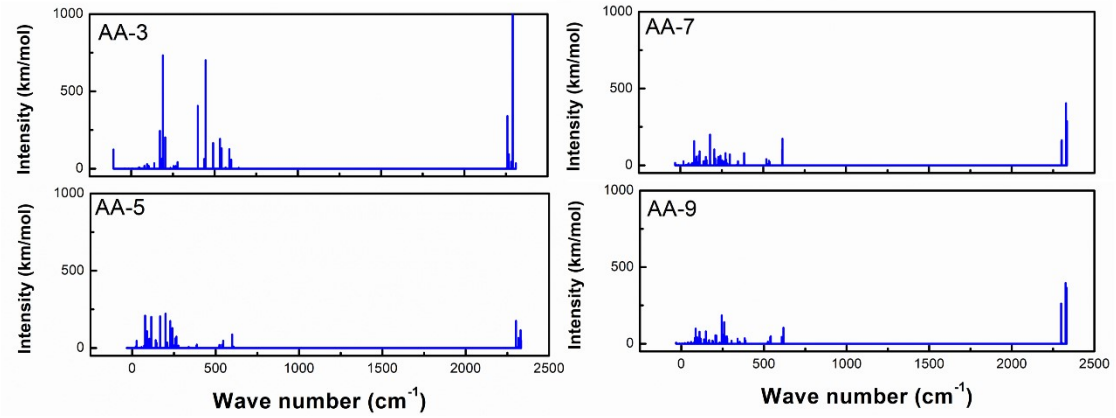


**Fig. S3.** Vibrational spectra of AA-$PdSe_2$ nanoribbons at Gamma point with varying width.

The stability sequence (SS > ZZ > ZA > AA) of the penta-$PdSe_2$ nanoribbons in our study is different from the results (ZZ > ZA > AA > SS) in reference [Surf. Sci. 2023, 728: 122206]. However, our result is consistent with the stability sequence of penta-graphene [Phys. Chem. Chem. Phys. 2017, 19: 9528–9536] and penta-$BN_2$ nanoribbons [Comput. Mater. Sci. 2021, 190: 110275]. There are two factors contributing to this stability sequence difference from [Surf. Sci. 2023, 728: 122206], i.e. edge passivation strategy and SS structural model.

[Surf. Sci. 2023, 728: 122206] employed a fractional charge pseudo-hydrogen atom passivation strategy to saturate the dangling bonds of the edge Pd/Se atoms (e.g., Z = 0.66 for Se-site pseudo-H, Z = 0.1 for Pd-site pseudo-H). This required custom modifications to the POTCAR pseudo-potential parameters of Pd, Se, and hydrogen atoms in VASP and the distinction of pseudo-hydrogen types in the POSCAR. In contrast, our study used a conventional direct hydrogen passivation method, which employed standard POTCAR pseudo-potentials and did not require any manual modifications. This passivation approach more closely resembles the common experimental environment for the preparation of low-dimensional nanoribbons and is consistent with the general computational studies on analogous materials such as penta-graphene [Phys. Chem. Chem. Phys. 2017, 19: 9528–9536], penta-$BN_2$ [Comput. Mater. Sci. 2021, 190: 110275], and penta-$SiC_2$ nanoribbons [Mater. Today Commun. 2021, 26: 102047].

The pseudo-H passivation strategy in [Surf. Sci. 2023, 728: 122206] is not a good choice for our study since we consider the change of widths. Because different edge widths require different fractional charges for pseudo-H atoms, the fractional charges of the pseudo-H atoms need to be re-optimized for different widths, which is difficult to achieve in our work.

On the other hand, the monolayer $PdSe_2$ structure shows anisotropy in different directions, as shown in Fig. S2(a). The SS structure we are studied is a nanoribbon with edges along the *x* direction where the side view is shown in Fig. S2(b). But the SS structure in [Surf. Sci. 2023, 728: 122206] is a nanoribbon along the *y* direction where the side view is shown in Fig. S2(c). Due to the anisotropy of the penta-$PdSe_2$ structure, the bond lengths differ along different directions. Along the x direction, the edge Pd-Se bond length is 2.468 Å and the Se-Se bond length is 2.423 Å; along the y direction, the edge Pd-Se bond length is 2.447 Å and the Se-Se bond length is 2.419 Å. Therefore, the stability of the SS structure in different edge direction can be different.

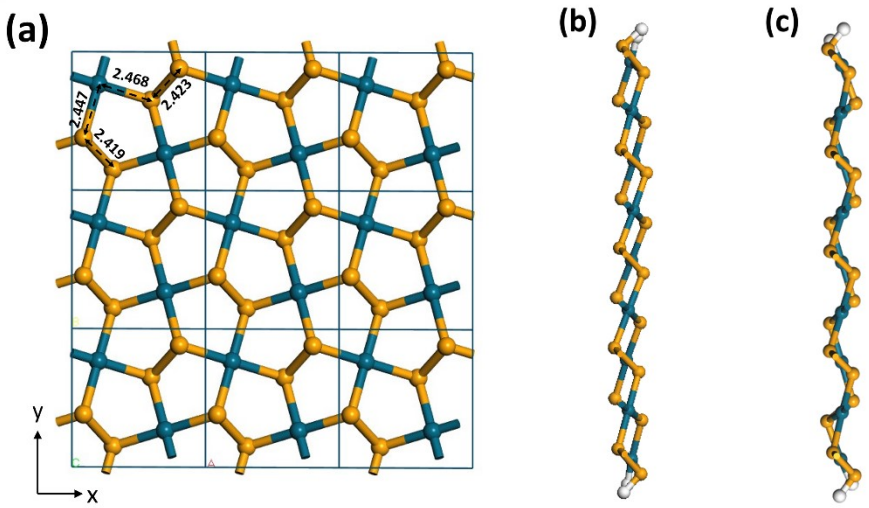


**Fig. S4.** (a) different bond lengths in *x*- and *y*- axis to show the anisotropy monolayer $PdSe_2$, where the blue dashed rectangle illustrates the SS nanoribbon (SS-*x*) in our work and the red rectangle illustrates the SS nanoribbon in [Surf. Sci. 2023, 728: 122206]. (b) the side view of SS-*x* nanoribbons in our work; and (c) the side view of SS-*y* nanoribbons in [Surf. Sci. 2023, 728: 122206].

To further verify the reliability of our predicted results, we performed PBE+U calculations including an onsite Hubbard *U* correction for the AA nanoribbons with widths from 3 to 9, as shown in the Fig. S5. Based on previous reports [npj Comput. Mater. 2025, 11: 18], we applied a *U* value of $U_{eff} = 4\ eV$ to the Pd-d orbitals. The results show that after introducing the *U* correction, the magnetic ground states for each width remain unchanged. The non-magnetic to antiferromagnetic to ferromagnetic transition with increasing width remains clearly evident at the PBE+*U* level. Therefore, the Hubbard *U* correction is not significant for the penta-$PdSe_2$ nanoribbons. Also, previous work on penta-$PdSe_2$ nanoribbons didn't consider the Hubbard *U* correction [Surf. Sci. 2023, 728: 122206].

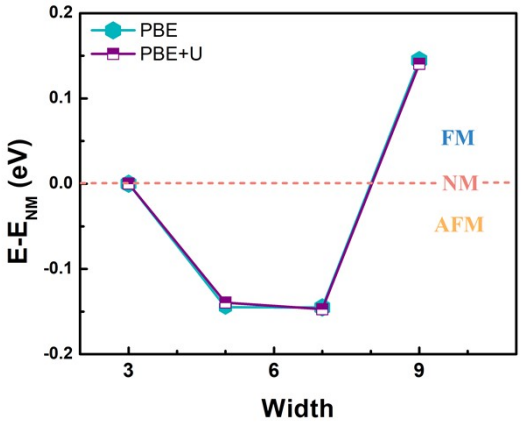


**Fig. S5.** Magnetic ground states of AA nanoribbons for the widths of 3, 5, 7 and 9, calculated with PBE and PBE+U.

Band gap comparison for narrowed AA and ZA nanoribbons calculated by PBE and HSE06 functional is presented. As expected, the PBE calculations distinctly underestimate the band gap, especially for the narrowed width. Despite the distinct underestimation of the band gap by the PBE functional, the underlying rules governing the dependence of band gap on width are consistent across both methods.

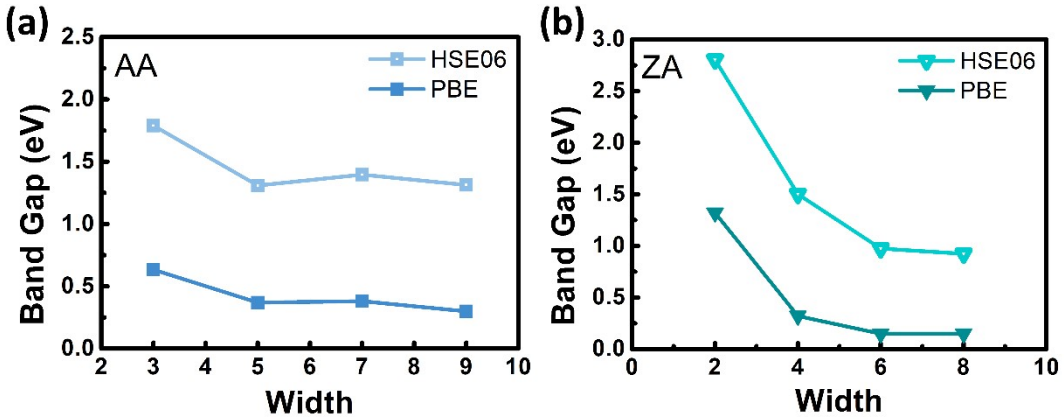


**Fig. S6.** Band gap of (a) AA and (b) ZA nanoribbons with narrowed widths, calculated by PBE and HSE06 functional separately.